X-ray Structures of the Myosin Motor Domain of *Dictyostelium discoideum* Complexed with MgADP·BeF_x and MgADP·AlF_4^- †,‡

Andrew J. Fisher,§ Clyde A. Smith,§ James B. Thoden,§ Robert Smith,§ Kazuo Sutoh,|| Hazel M. Holden,§ and Ivan Rayment*,§

Institute for Enzyme Research and Department of Biochemistry, University of Wisconsin, Madison, Wisconsin 53705, and Department of Pure and Applied Sciences, University of Tokyo, Komba, Tokyo 153, Japan

Received March 15, 1995; Revised Manuscript Received May 3, 1995⊗

ABSTRACT: The three-dimensional structures of the truncated myosin head from *Dictyostelium discoideum* myosin II complexed with beryllium and aluminum fluoride and magnesium ADP are reported at 2.0 and 2.6 Å resolution, respectively. Crystals of the beryllium fluoride−MgADP complex belong to space group $P2_12_12$ with unit cell parameters of a = 105.3 Å, b = 182.6 Å, and c = 54.7 Å, whereas the crystals of the aluminum fluoride complex belong to the orthorhombic space group $C222_1$ with unit cell dimensions of a = 87.9 Å, b = 149.0 Å, and c = 153.8 Å. Chemical modification was not necessary to obtain these crystals. These structures reveal the location of the nucleotide complexes and define the amino acid residues that form the active site. The tertiary structure of the protein complexed with MgADP·BeF_x is essentially identical to that observed previously in the three-dimensional model of chicken skeletal muscle myosin subfragment-1 in which no nucleotide was present. By contrast, the complex with MgADP·AlF_4^- exhibits significant domain movements. The structures suggest that the MgADP·BeF_x complex mimics the ATP bound state and the MgADP·AlF_4^- complex is an analog of the transition state for hydrolysis. The domain movements observed in the MgADP·AlF_4^- complex indicate that myosin undergoes a conformational change during hydrolysis that is not associated with the nucleotide binding pocket but rather occurs in the COOH-terminal segment of the myosin motor domain.

The molecular mechanism by which chemical energy is transduced into directed movement is a fundamental question in biology. It is well established that muscle contraction occurs when the thick and thin filaments, which are built primarily of myosin and actin, slide past each other (Huxley & Niedergerke, 1954; Huxley & Hanson, 1954). Movement occurs through the interaction of the globular head of myosin with actin and is driven by the hydrolysis of ATP.

Recently, the three-dimensional structures of both actin and myosin were determined by X-ray crystallography (Holmes et al., 1990; Kabsch et al., 1990; Rayment et al., 1993b), and combination of these results with those from electron microscopy gave rise to a structural hypothesis for how myosin converts chemical energy into directed movement (Milligan & Flicker, 1987; Milligan et al., 1990; Rayment et al., 1993a). The major tenet of this hypothesis was that domain movements in myosin, induced by the binding of ATP to the actin-bound state, generate a cyclical series of conformational changes that reduce the affinity of myosin for actin and place the myosin in a state in which it can hydrolyze the nucleotide. Movement of myosin relative to actin was suggested to occur through reversal of the induced conformational changes as myosin rebinds to actin and releases the reaction products. This model was consistent with previous kinetic studies, both in solution and in fibers, which have established that the power stroke, or energy transduction process, occurs during product release (Goldman, 1987; Lymn & Taylor, 1971). Central to this hypothesis was the suggestion that myosin interacts with actin in a stereospecific manner such that the onset of binding requires the molecules to be in a unique orientation before the power stroke is initiated. This hypothesis left questions unanswered concerning the nature of the structural transitions that underlie this process and the mechanism of ATP hydrolysis.

One of the most important questions raised by the initial model of myosin subfragment-1 (myosin S1)[1] was what is the structure of the myosin head with ATP bound? It was suggested that the nucleotide binding pocket closes when ATP binds to myosin and generates a large movement of the COOH terminus of the myosin head relative to the actin binding conformation (Rayment et al., 1993a). This change would then prepare the molecule to unbend as it reattached to actin and to release the products of hydrolysis. Given the complexity of the myosin head, it was impossible to

† This work was supported by NIH Grant AR35186 to I.R. C.A.S. is a Fogarty International Research Fellow (TW05194). A.J.F. and J.T. are supported by NSRA Fellowships AR08304 and GM15950, respectively. K.S. is supported by a grant-in-aid from the Minister of Education, Science and Culture (06404081) and the Mitsubishi Foundation and the Ueha Memorial Foundation.

‡ The coordinates have been deposited in the Brookhaven Protein Data Bank (file names 1MMD and 1MND).

* Address correspondence to this author at the Institute for Enzyme Research, University of Wisconsin, 1710 University Ave., Madison, WI 53705.

§ University of Wisconsin.

|| University of Tokyo.

⊗ Abstract published in *Advance ACS Abstracts,* July 1, 1995.

[1] Abbreviations: myosin S1, myosin subfragment-1; S1Dc, *Dictyostelium discoideum* myosin II motor domain; PMSF, phenylmethanesulfonic acid; S1Dc·BeF_x·MgADP, the beryllium fluoride−ADP complex of *D. discoideum* myosin head; S1Dc·AlF_4·MgADP, the aluminum fluoride−ADP complex of *D. discoideum* myosin head; BTP, Bis-Tris-propane; DTT, dithiothreitol; HEPES, *N*-(2-hydroxyethyl)piperazine-*N*′-2-ethanesulfonic acid; rms, root mean square; P_i, phosphate; EDTA, ethylenediaminetetraacetic acid.

0006-2960/95/0434-8960$09.00/0

predict or model accurately the nature of these conformational changes.

Another question arose from the strategy adopted to obtain crystals of chicken skeletal myosin S1 (Rayment et al., 1993b). In that study it was found necessary to reductively methylate the protein in order to grow crystals suitable for structural analysis (Lundblad, 1991; Means & Feeney, 1968). Myosin retains its enzymatic activity after this modification even though many of the rate constants associated with the steps in the hydrolytic process are altered (White & Rayment, 1993). Control studies, in which the structure of hen egg white lysozyme was determined after chemical modification, revealed that reductive methylation had minimal effect on its tertiary structure (Rypniewski et al., 1993). It remained to be determined, however, whether the reductive alkylation had significantly altered the relative arrangement of domains within myosin. Recently, the use of the X-ray structure as a model for the contractile cycle has been questioned due to the changes in the enzymatic properties of the molecule induced by reductive methylation (Bivin et al., 1994; Phan et al., 1994).

Questions concerning the structure of the myosin head also remained unanswered because the original structure determination was only at 2.8 Å resolution. Although this revealed the path of the polypeptide chain, it was not of high enough resolution to categorically define the geometry of all of the important residues in the active site or the water structure. Identification of the hydrogen-bonding patterns and the water structure within the active site is critical, since hydrolysis occurs by attack of a water molecule on the γ-phosphorus atom of ATP. The restricted quality of the diffraction from the crystals arose not only from the numerous myosin heavy and light chain isoforms and from the proteolytic heterogeneity introduced in their preparation but also from its asymmetric shape.

The questions outlined above can be addressed only by determination of the structure of the myosin head in presence of an ATP analog, without chemical modification, and from a crystal form that diffracts to higher resolution. Chemical studies have shown that it is possible to trap ADP in the active site of myosin in a variety of ways including cross-linking the two reactive sulfydryl groups in the myosin heavy chain and through the formation of long-lived complexes of ADP with phosphate analogs. These studies have proved to be of enormous value in dissecting the catalytic cycle and defining the environment of the active site (Yount et al., 1992). Phosphate analogs include vanadate (Goodno, 1982) and more recently beryllium fluoride and aluminum fluoride (Phan & Reisler, 1992; Phan et al., 1993; Werber et al., 1992). It has been suggested that these complexes are analogs of the metastable ADP,P_i state that occurs after hydrolysis (Maruta et al., 1993; Phan et al., 1993). The beryllium and aluminum fluoride complexes are of particular interest since they are very stable and thus are good candidates for structural studies (Maruta et al., 1993). We report here the structures of the MgADP complexes of the motor segment of myosin II from *Dictyostelium discoideum* in the presence of beryllium and aluminum fluoride at 2.0 and 2.6 Å resolution, respectively. These structures suggest that the MgADP•BeF_x complex mimics the ATP bound state and the MgADP•AlF_4^- complex is an analog of the transition state for hydrolysis. Myosin from *Dictyostelium discoideum* was chosen for this study since an expression system for chicken skeletal muscle myosin was not available.

EXPERIMENTAL PROCEDURES

Protein Design and Purification. The myosin head is a highly asymmetric molecular assembly (Rayment et al., 1993b). It is characterized by a cluster of domains that define a motor unit, which is attached to an extended motif where the myosin light chains bind. The motor unit in skeletal muscle myosin is built from approximately 780 amino acid residues. The light chain binding motif, also called the regulatory domain (Xie et al., 1994), is built around an 85 Å long α-helix that leaves the motor unit and extends throughout the remainder of the myosin head. The three-dimensional structure of the isolated light chain binding motif in scallop has been determined independently and confirms that observed in chicken skeletal myosin S1 (Xie et al., 1994). Examination of the myosin head suggested it might be possible to generate a shorter head that contained all of the elements of the molecular motor and might be more suitable for crystallization. This has been accomplished by expression of a truncated head from the myosin II of *D. discoideum* (Itakura et al., 1993) with the system developed by Spudich and co-workers (Manstein et al., 1989). This truncated head retains its ATPase activity although the kinetic rate constants have changed (Sally Woodward, personal communication). It also exhibits a limited ability to move actin, suggesting that it contains the fundamental unit necessary to generate movement (Itakura et al., 1993).

The myosin heavy chain was truncated genetically at residue Ile 762 to yield a fragment with molecular weight ~87 kDa. The site of truncation was equivalent to residue Leu 783 in chicken skeletal muscle myosin. The fragment studied here consists of residues Asp 2 to Asn 762 in the sequence of *Dictyostelium* myosin (Warrick et al., 1986). It is presumed that the initial methionine has been removed since no density is observed for this residue. In the original sequence the second amino acid was an asparagine residue. This was converted to an aspartate during the construction of the fragment. The side chain of Asp 2 forms a salt bridge to Arg 146 in a manner that is consistent with this amino acid. Additionally, the final three residues were changed from Gln-Arg-Ile in the original sequence to Leu-Pro-Asn to create a restriction site (Itakura et al., 1993). The motor unit of *Dictyostelium* myosin is smaller than that of chicken skeletal muscle myosin due to shorter loops that connect the major tryptic fragments (Balint et al., 1975; Mornet et al., 1979; Warrick et al., 1986).

The truncated myosin head from *D. discoideum* (S1Dc) was prepared as before with modifications (Itakura et al., 1993). The *Dictyostelium* cells were grown in axenic culture (HL5 medium) and harvested at saturation (1-2 × 10^7 cells/mL) by centrifugation. The cells were washed in 10 mM Tris, pH 8, and then frozen in liquid N_2. The isolation of the protein was carried out at 4 °C. Approximately 50 g of cells was resuspended by sonication in 400 mL of 20 mM Bis-Tris-propane (BTP), pH 7.5, 25 mM NaCl, 4 mM EDTA, 1 mM DTT, and 0.2 mM phenylmethanesulfonyl fluoride (PMSF). The cellular debris was removed by centrifugation at 1000*g* for 10 min, whereupon the cytoskeletal components were collected by a high-speed centrifugation at 235 000*g* for 1 h. The myosin was extracted from the pellets by the

Table 1: X-ray Data Collection Statistics

complex	source and detector	λ	T (°C)	total unique	redundancy	completion (%)	resolution (Å)	R_{merge}[a]
MgADP·BeF_x·S1Dc	Siemens HI-STAR	1.542	4	32 930	2.5	98	2.6	11.0
MgADP·BeF_x·S1Dc	SSRL, MAR scanner	1.08	4	63 717	6.3	88	2.0	3.3
MgADP·AlF_4·S1Dc	Siemens	1.542	−160	29 506	2.3	96	2.6	6.1

[a] $R_{merge} = \Sigma\Sigma\{||I_{hi}| - |I_h||\}/\Sigma_{hi}I_{hi} \times 100$, where I_{hi} and I_h are the intensities of the individual and mean structure factors.

addition of 20 mM BTP at pH 7.5, 50 mM NaCl, 7 mM $MgCl_2$, 6 mM ATP, 1 mM DTT, and 0.2 mM PMSF. The actin and other cytoskeletal components were removed by centrifugation at 250 000*g* for 80 min. The supernatant was applied to a 50 mL Toyopearl DEAE-650M column to remove any residual actin. S1Dc was precipitated by the addition of solid ammonium sulfate to 70% saturation. The precipitate was recovered by centrifugation and dialyzed against 50 mM Tris-HCl, pH 8.0, containing 100 mM KCl, 2 mM $MgCl_2$, 0.2 mM NaN_3, 1 mM DTT, and 0.2 mM PMSF. The resultant solution was clarified by centrifugation and applied to an ATP affinity column where the attachment of the nucleotide to the column substrate was via the ribose 2′- or 3′-hydroxyl group (synthesized by Ralph Yount, Washington State University). S1Dc was eluted with 50 mM Tris-HCl at pH 8.0 containing 100 mM KCl, 2 mM sodium pyrophosphate, 2 mM EDTA, 0.2 mM NaN_3, and 1 mM DTT. The protein was concentrated to 8−10 mg/mL by microfiltration and exchanged simultaneously into 10 mM HEPES, pH 8.0, 100 mM NaCl, 2 mM $MgCl_2$, 0.2 mM NaN_3, and 1 mM DTT. A typical preparation yields 3 mg of protein from 50 g of cells.

Crystal Growth. Crystals of the beryllium fluoride−magnesium ADP complex with S1Dc were grown by microbatch from a mixture of final composition 4−5 mg/mL protein, 8.5% poly(ethylene glycol) 8000, 25 mM HEPES pH 7.0, 1.5% methylpentanediol, 170 mM NaCl, 1.8 mM ADP, 1.8 mM $MgCl_2$, 1.8 mM $BeCl_2$, 9 mM NaF, and 3 mM DTT at 4 °C. The crystals of the aluminum fluoride complex were grown under similar conditions except that the beryllium chloride was replaced by 1.75 mM $Al(NO_3)_3$ and the sodium fluoride concentration lowered to 6 mM. Crystallization was induced by the introduction of either micro- or macroseeds obtained from preliminary hanging-drop experiments. The protein was not chemically modified.

X-ray Data Collection and Processing. Crystals of the beryllium fluoride−MgADP complex (MgADP·BeF_x·S1Dc)[2] belong to space group $P2_12_12$ with unit cell parameters of a = 105.3 Å, b = 182.6 Å, and c = 54.7 Å. There is one molecule per asymmetric unit (V_M = 3.0 Å^3/Da, solvent content ≈ 59%). These crystals show diffraction to 1.8 Å resolution with synchrotron radiation, although data to 2.0 Å resolution were utilized in the present study. An initial X-ray data set was recorded on a Siemens HI-STAR double-detector system at 4 °C and extended to higher resolution at the Stanford Synchrotron facility (SSRL) with a MAR image plate detector. In contrast, crystals of the aluminum fluoride complex (MgADP·AlF_4·S1Dc) belong to the orthorhombic space group $C222_1$ with unit cell dimensions of a = 87.9 Å, b = 149.0 Å, and c = 153.8 Å. The crystals contain one molecule per asymmetric unit (V_M = 2.9 Å^3/Da, solvent content ≈ 58%). X-ray data were collected from a single crystal at −160 °C on a Siemens HI-STAR area detector. A summary of the data collection statistics is reported for both crystal forms in Table 1.

Structure Determination of MgADP·BeF_x·S1Dc. The structure of MgADP·BeF_x·S1Dc was solved by molecular replacement from a phasing model based on the chicken myosin S1 structure composed of residues Glu 74 to Glu 776 (Rossmann, 1972). This excluded the NH_2-terminal β-barrel and the light chain binding motif. All the nonconserved residues were truncated to alanines in the chicken S1 search model. Area detector data between 9.0 and 4.5 Å resolution were used in a Patterson correlation refinement of the 51 strongest rotation peaks (Brünger, 1990a,b) and generated a single peak which was 2.3σ greater than the next highest peak. The highest peak in the translation search (1.3σ greater than the next highest) gave in an R-factor of 49.3% for all data to 3.5 Å resolution. Identical solutions were obtained with the molecular replacement programs GLRF and AMORE (Navaza, 1993; Tong & Rossmann, 1990). The phasing model was divided into five components that were allowed to vary independently during rigid body refinement. This decreased the R-factor to 44.7%. An initial electron density map was computed using SIGMAA coefficients to suppress the model bias (Read, 1986) and revealed density for most of the side chains that were excluded from the phasing model as well as strong density for the MgADP·BeF_x complex. In the initial map most of the residues between Asp 75 and Ile 696 were visible. A few strands were observed for the NH_2-terminal β-barrel domain. The last residue observed at the carboxyl-terminal end was Ile 696. After the first round of model building, the structure was refined by the simulated annealing algorithm in X-PLOR (Brünger, 1990b) followed by conventional least squares refinement with the program TNT (Tronrud et al., 1987). This reduced the R-factor to 35.0% for all recorded data to 2.7 Å resolution. Thereafter, the model was refined against the synchrotron data (SSRL) to 2.0 Å resolution. After refinement the final model included 743 residues together with 375 water molecules and the nucleotide complex. The final R-factor between the observed and calculated data was 19.1% for all data recorded between 30 and 2.0 Å resolution where the rms deviation from ideality for the bond lengths, angles, and trigonal planes was 0.015 Å, 2.26°, and 0.007 Å, respectively. A section of representative electron density for the protein and the nucleotide complex in the active site pocket is shown in parts a and b of Figure 1, respectively.

Structure Determination of MgADP·AlF_4·S1Dc. The aluminum fluoride complex was solved by molecular replacement (Rossmann, 1972) from the structure of MgADP·BeF_x·S1Dc and refined in a similar manner. Data between 10.0 and 4.0 Å were included in the rotation and translation searches. A Patterson correlation refinement of the overall orientation and of the individual orientations of five fragments of the S1 model was performed on the top 200 peaks

[2] The exact composition of the beryllium fluoride species is unknown (Henry et al., 1993; Maruta et al., 1993). Consequently, these complexes will be designated as BeF_x and AlF_4^-.

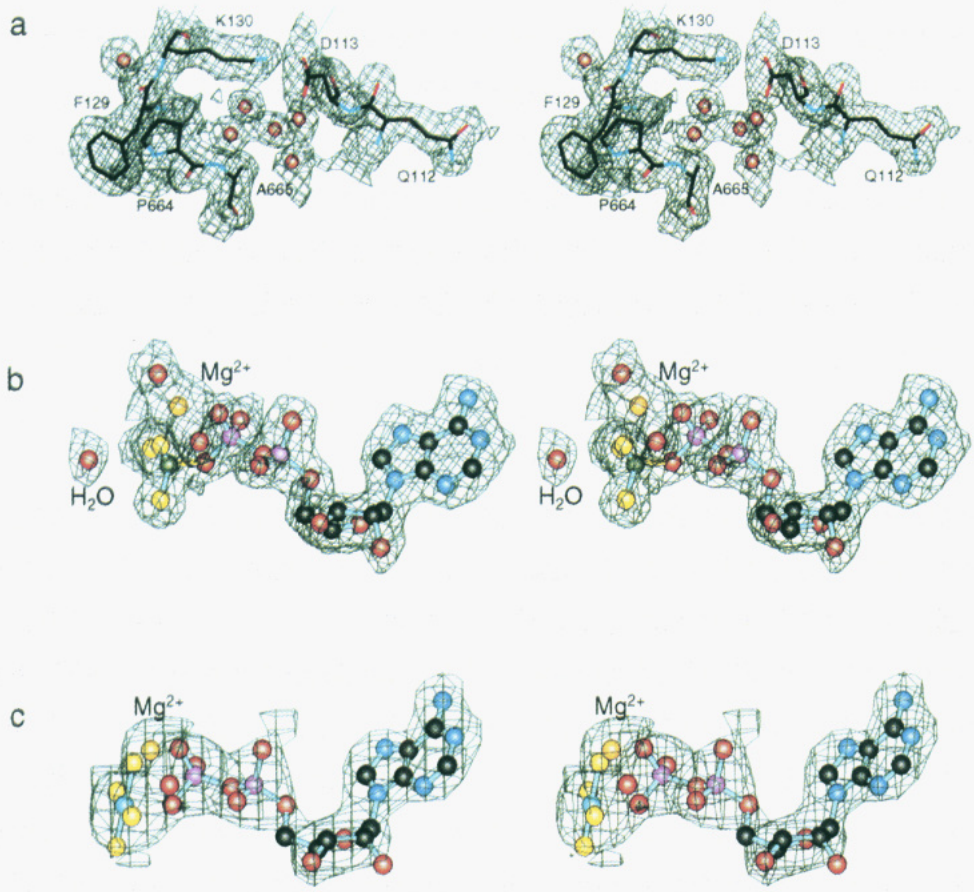

FIGURE 1: (a) Representative electron density for a segment including Lys 130 near the active site pocket in the MgADP·BeF_x·S1Dc complex at 2.0 Å resolution. (b) Electron density for the nucleotide complex in the active site pocket of the MgADP·BeF_x·S1Dc complex. (c) Electron density for the MgADP·AlF_4·S1Dc complex. In (b) and (c) aluminum, beryllium, carbon, fluorine, magnesium, nitrogen, oxygen, and phosphorus are depicted in cyan, green, black, yellow, orange, blue, red, and pink, respectively. The majority of the electron density in the central segment of the myosin heavy chain is of this quality in the MgADP·BeF_x·S1Dc complex. Although the protruding NH_2-terminal domain and the COOH-terminal domain in the MgADP·BeF_x·S1Dc structure have higher temperature factors, the chain tracing is unequivocal. Although the density for the AlF_4^- complex appears spherical, when these atoms are excluded from the phase calculation the difference density is clearly square planar, providing definitive positions for the fluorine ligands. This figure was prepared from a plot file generated from the molecular graphics program FRODO (Jones, 1985) and drawn with the program MOLVIEW (Smith, 1993). A cover radius of 2.0 Å was chosen to exclude density not associated with the atoms shown.

from the rotation search. Several strong solutions emerged from the Patterson correlation refinement, all of which were close to the highest peak. A translation search with this orientation yielded a peak 6σ greater than the next highest, with an R-factor of 48.7%. After rigid-body refinement of the whole search model and the five fragments the initial electron density map revealed the location of the MgADP and the AlF_4^- moiety. Further refinement with simulated annealing reduced the R-factor to 31% (Brünger, 1990b). Additional conventional least squares refinement revealed the location of the NH_2-terminal domain (Brünger, 1990b; Tronrud et al., 1987). There are breaks in the polypeptide chain between Gln 19 and Leu 27, Ala 205 and Gly 209, Phe 487 and Leu 508, Arg 620 and Asn 626, and Glu 681 and Gly 683, where the density is poorly defined. A total of 646 residues was included in the present model together with 104 water molecules and the nucleotide complex. The final R-factor between the observed and calculated data was 24.2% for all data between 30 and 2.6 Å resolution where the rms deviation from ideality for the bond lengths, angles, and trigonal planes was 0.013 Å, 2.39°, and 0.016 Å, respectively. Most of the residues between Asp 2 and Lys 690 are well defined; however, the COOH-terminal 70 residues appear to adopt multiple conformations in the crystal and have not been modeled at present. In both structures, almost all of the non-glycinal residues lie within the fully allowed regions of the Ramachandran plot (Figure 2). The few exceptions lie either in loops or at crystal contacts.

RESULTS AND DISCUSSION

Tertiary Structure of MgADP·BeF_x·S1Dc. The tertiary structure of the beryllium fluoride complex is described first because it most closely matches that of chicken skeletal muscle myosin S1 and because it is a more complete model. The overall topology of the protein will be described with respect to the three major tryptic fragments of skeletal muscle myosin S1, the NH_2-terminal 25 kDa, the central 50 kDa, and the COOH-terminal 20 kDa fragment (Balint et al., 1975; Cooke, 1986; Mornet et al., 1979).

A ribbon drawing of the MgADP·BeF_x·S1Dc complex is shown in Figure 3, where the molecule is oriented to view into the narrow cleft that splits the central 50 kDa segment of the myosin heavy chain. A comparison of the chicken and *Dictyostelium* myosin heads is shown in Figure 4a. The overall domain structure and topology of the truncated head of *Dictyostelium* myosin is remarkably similar to that of the chicken skeletal muscle myosin S1 with which it shares 47% sequence identity (Warrick et al., 1986). The rms difference

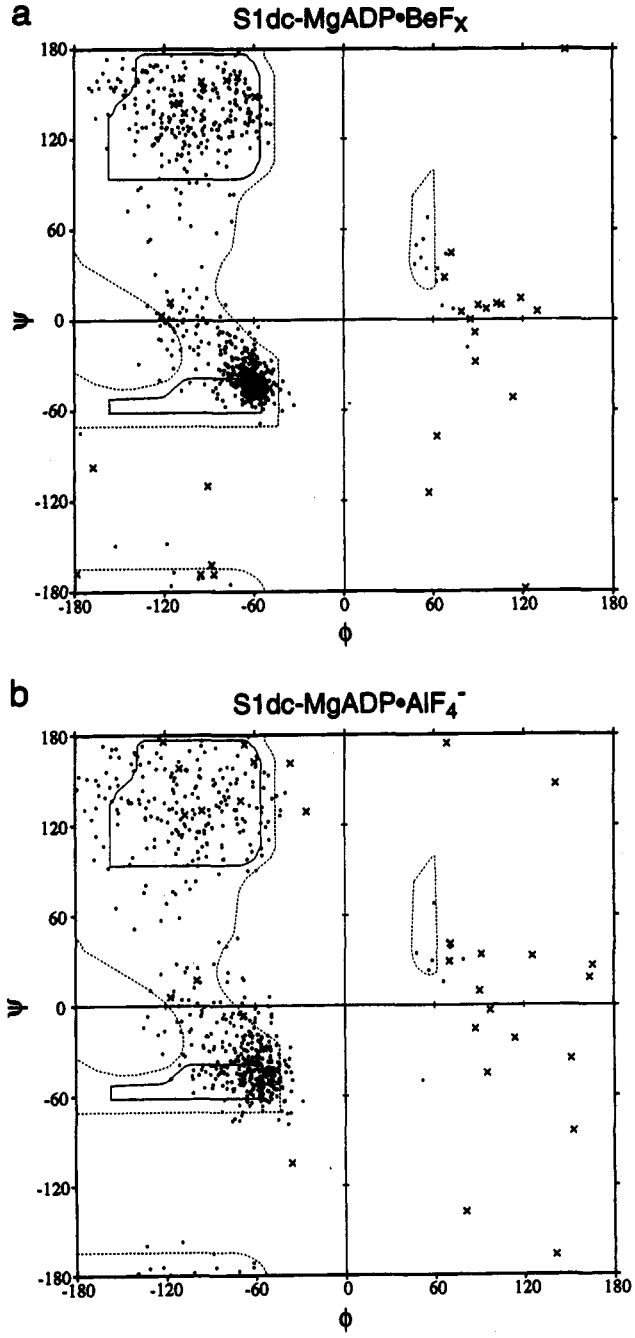

FIGURE 2: Ramachandran plot of the main-chain dihedral angles for (a) MgADP•BeF_x•S1Dc and (b) MgADP•AlF_4•S1Dc. All non-glycinal dihedral angles are indicated as dots whereas the glycinal angles are shown as crosses. Fully allowed ϕ and ψ values are enclosed by continuous lines; those only partially allowed are enclosed by broken lines.

between 554 equivalent α-carbons in chicken and *Dictyostelium* myosin is 1.25 Å. This is only slightly larger than the expected difference of 1.1 Å for proteins that share the same function and exhibit 47% sequence identity (Chothia & Lesk, 1986). A comparison of the rms differences between both of the metallofluoride−ADP complexes of S1Dc and chicken skeletal muscle myosin S1 is given in Table 2. The NH_2- and COOH-terminal regions of the *Dictyostelium* myosin sequence were excluded from the initial refinement and were built independently of the known fold for chicken myosin S1. Although there is limited sequence identity in these regions, the similarity in topology is consistent with the conserved function (Chothia & Lesk, 1986) and thus serves to confirm both the chicken and *Dictyostelium* chain tracings. The structural similarity seen here proves that reductive methylation found necessary to obtain crystals of chicken S1 (Rayment et al., 1993b) did not alter the domain structure of the myosin head. It is noteworthy that the narrow cleft that splits the 50 kDa segment of the heavy chain is equally open in both chicken and MgADP•BeF_x•S1Dc structures. Contrary to expectations, the nucleotide binding pocket in MgADP•BeF_x•S1Dc has only closed about 1 Å relative to that observed in the chicken skeletal myosin S1.

In the MgADP•AlF_4•S1Dc complex, the tertiary structures of the individual domains that form the NH_2-terminal, upper and lower central segments and COOH-terminal segments of the heavy chain are very similar to those of the MgADP•BeF_x•S1Dc complex (Table 2). However, the relationship between the domains has changed (Figure 4b). The most obvious difference is the partial closure of the cleft that splits the central segment of the myosin heavy chain. This results in a significant rearrangement of the COOH-terminal segment of the polypeptide chain beyond Lys 690. The reason for this conformational change originates in difference in the coordination of the beryllium and aluminum fluoride moieties in the phosphate binding pocket. The final segment of the model includes Cys 678 and Thr 688 that are equivalent to the reactive cysteine residues (SH2 and SH1) in skeletal muscle. Even though Cys 678 and Thr 688 are still located at opposite ends of an α-helix as observed in chicken myosin subfragment-1 (Rayment et al., 1993b), the orientation of the helix has changed by ~20°. The significance of this movement is discussed briefly later. However, due to the disorder present in the MgADP•AlF_4•S1Dc complex the discussion of these structures will focus on the catalytic mechanism for ATP hydrolysis.

Structure of the Adenine and Ribose Binding Pocket. The nucleotide binding site lies at the base of a pocket formed on one side by residues from the NH_2-terminal segment of the myosin heavy chain and on the other by residues from the central section as indicated in Figure 3 and shown in detail in Figure 5. There is well defined electron density in both the MgADP•BeF_x•S1Dc and MgADP•AlF_4•S1Dc complexes for ADP, the metallofluoride complex, a magnesium ion, and several water molecules in the nucleotide binding pocket (Figure 1b,c). The coordination of the adenine and ribose is essentially identical in both complexes. Consequently, the discussion of this component of the nucleotide binding site will be described relative to the structure of MgADP•BeF_x•S1Dc since this is the better model.

In both complexes the purine ring is in the anti conformation relative to the ribose, which exhibits a C3′-endo ring pucker. Almost all of the residues involved in the binding of the nucleotide lie above the plane of the β-sheet that forms the major tertiary structural motif in the myosin head. However, the pocket extends down into the opening between the cleft that splits the upper and lower domains of the central 50 kDa segment. A schematic drawing of the myosin−nucleotide interactions in the MgADP•BeF_x•S1Dc complex is shown in Figure 6. The binding site for the purine ring in both complexes is formed almost exclusively from residues in the NH_2-terminal segment of the chain. It lies in a small indentation formed on one side by the first turn of the helix that follows the characteristic phosphate binding-loop sequence (Walker et al., 1982) and involves residues Gly 184,

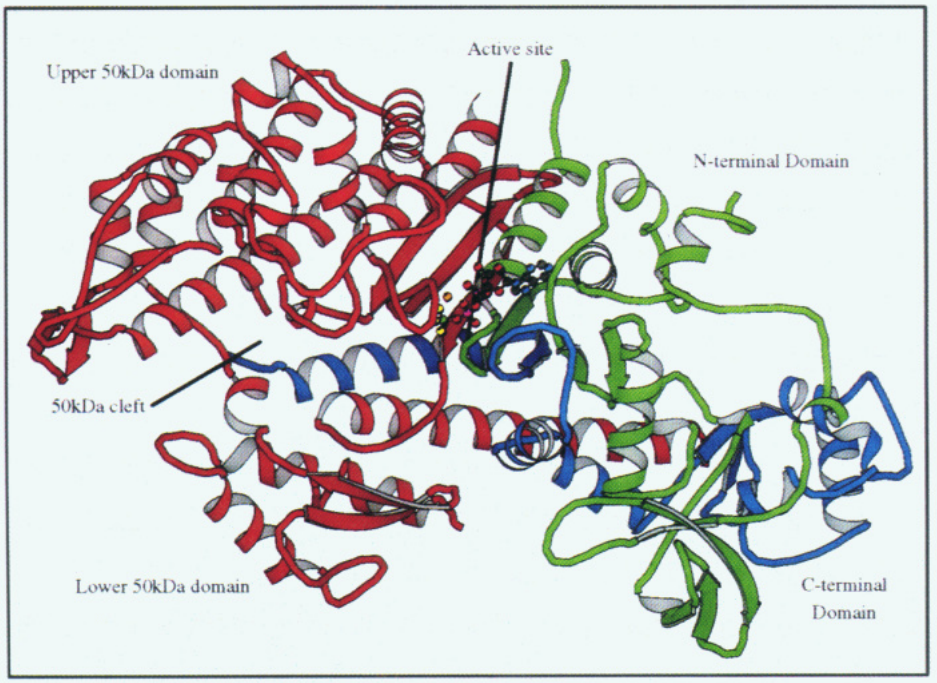

FIGURE 3: Ribbon representation of the MgADP•BeF_x•S1Dc complex of the truncated *Dictyostelium* myosin. The heavy chain is displayed in green, red, and blue to delineate the NH_2-terminal, central, and COOH-terminal fragments that extend from residues Asn 2 to Ala 205, Gly 209 to Ala 621, and Phe 627 to Ala 759, respectively. These segments are separated by loops for which the electron density is ill-defined. In addition to the short loops that connect these segments, residues Thr 501 to Gly 507 are disordered. This figure and figures 4, 5, and 7 were prepared with the molecular graphics program MOLSCRIPT (Kraulis, 1991).

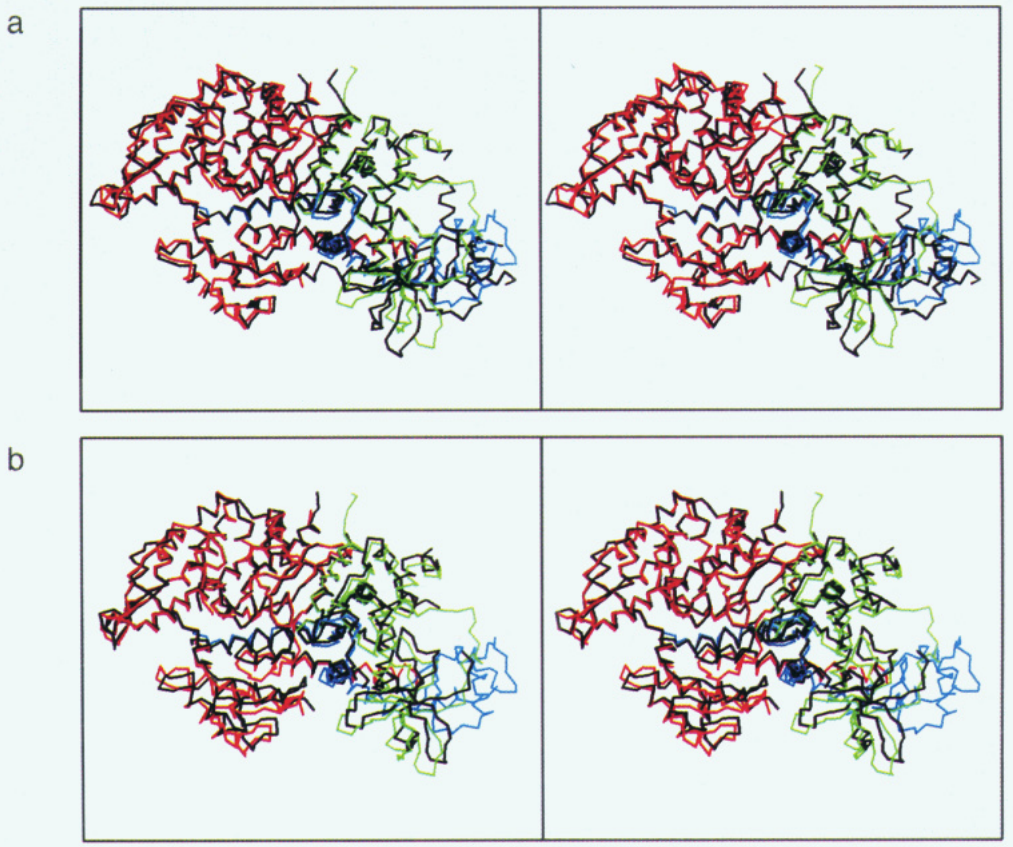

FIGURE 4: Stereo α-carbon plots of the alignment of the motor units of (a) chicken skeletal muscle myosin and the MgADP•BeF_x•S1Dc complex of *Dictyostelium* myosin and (b) MgADP•BeF_x•S1Dc and MgADP•AlF_4•S1Dc complexes of *Dictyostelium* myosin. The MgADP•BeF_x•S1Dc structure is shown in green, red, and blue to distinguish the NH_2-terminal, central, and COOH-terminal segments of the myosin heavy chain. In (a) and (b) the structures of chicken skeletal muscle myosin S1 and MgADP•AlF_4•S1Dc are shown in black, respectively.

Glu 187, and Asn 188. The other side of the indentation is built from the strand that forms the top of one side of the nucleotide binding pocket and includes contributions from Asn 127, Pro 128, Arg 131, and Tyr 135. Arg 131 folds over the purine ring, protecting it from external solvent, and forms a salt bridge with Glu 187. In many myosins Arg 131 and Glu 187 are a tryptophan and valine, respectively. The equivalent tryptophan residue in skeletal muscle myosin

Table 2: rms Differences (Å) between Structurally Equivalent α-Carbon Positions in Chicken Skeletal Myosin Subfragment-1 and the MgADP·BeF_x·S1Dc and MgADP·AlF_4·S1Dc Complexes[a]

	N-terminal domain	upper 50 kDa domain	lower 50 kDa domain	C-terminal domain	whole molecule
MgADP·BeF_x·S1Dc onto chicken S1	0.73 (117)	1.20 (225)	0.89 (118)	1.15 (109)	1.25 (554)
MgADP·AlF_4·S1Dc onto chicken S1	0.95 (117)	1.25 (225)	1.33 (116)	1.42 (49)	1.91 (504)
MgADP·BeF_x·S1Dc onto MgADP·AlF_4·S1Dc	0.62 (186)	0.63 (244)	0.91 (132)	0.99 (54)	1.51 (640)

[a] The numbers of structurally equivalent α-carbon atoms used in the superposition calculation are given in parentheses. Surface loops which showed large deviations in α-carbon positions were omitted from the calculations. The structures have been divided into four parts representing the NH_2-terminal domain, the upper and lower domains of the central 50 kDa segment, and the COOH-terminal domain. In the whole molecule superpositions between the chicken structure and the two *Dictyostelium* structures, the first 84 residues of the N-terminus were omitted due to large differences in the trace of the polypeptide chains. In addition, the last 60 residues of the C-terminal region have also been omitted in the chicken–MgADP·BeF_x·S1Dc superposition, as the polypeptide chains are in a slightly different location even though they have an almost identical fold.

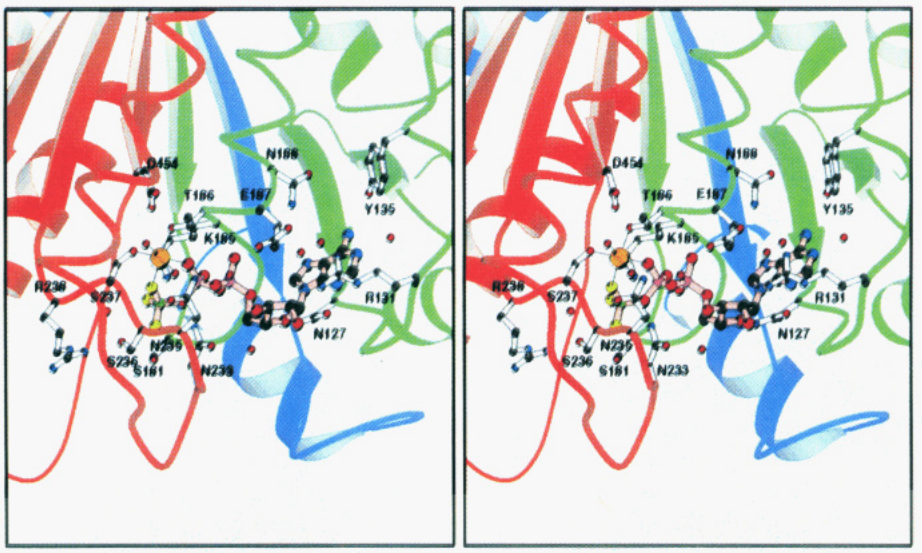

FIGURE 5: Stereo ribbon representation view of the nucleotide binding region of the MgADP·BeF_x·S1Dc complex. The tertiary structure is shown in green, red, and blue to distinguish the NH_2-terminal, central, and COOH-terminal segments of the myosin heavy chain. This reveals the orientation of the nucleotide and its associated magnesium ion. The phosphate binding site is located in the middle of the large β-sheet that forms the major structural motif in the myosin head and lies at the COOH-terminal end of the central β-strand. In this figure the MgADP·BeF_x is drawn with pink bonds, beryllium in green, carbon in black, fluorine in yellow, Mg^{2+} in orange, nitrogen in blue, oxygen in red, H_2O in red, phosphorus in magenta, and side chains that interact with the nucleotide with white bonds.

has been identified to be in the nucleotide binding site by photolabeling (Yount et al., 1992). There is a hydrogen bond between N6 of the purine and Oη of Tyr 135, which is a highly conserved residue. Although there are several buried water molecules that form hydrogen bonds between the purine and protein, there are very few other specific contacts between the purine ring and the protein. This is consistent with the observation that myosin will utilize a wide range of nucleotides and organic triphosphates albeit with varied kinetic and mechanical efficiency (Pate et al., 1993; White et al., 1993). The lack of specificity contrasts with the G-proteins or other ATP-dependent enzymes that utilize a phosphate binding loop (Muller & Schulz, 1992; Pai et al., 1990). However, this is consistent with the primary function of the myosin motor domain to convert the energy from hydrolysis of a phosphate bond into mechanical work.

Lys 130 in *Dictyostelium* myosin is not involved in any aspect of nucleotide binding. In the structure of chicken skeletal myosin this residue faces away from the active site pocket, whereas in *Dictyostelium* myosin this residue forms a salt bridge with Asp 113, which also lies outside the nucleotide binding pocket. The latter residue is not highly conserved across the myosin superfamily, which suggests the salt bridge is not a conserved feature of the myosin molecule. In most skeletal muscle myosins examined Lys 130 is trimethylated. In many other myosins the equivalent residue is an arginine. It has been suggested that since both trimethylated lysine and arginine would be expected to carry a constitutive positive charge, they might be involved in salt links to the phosphate groups of the nucleotide (Tong & Elzinga, 1983). In the structure of chicken skeletal muscle myosin this residue is clearly trimethylated (Rayment et al., 1993b), whereas in *Dictyostelium* myosin no density for the three additional methyl groups is evident (Figure 1a). At this time it is not clear what role this residue plays in the contractile mechanism. Site-directed mutagenesis of *Dictyostelium* myosin shows that conversion of this residue to a leucine generates a molecule with increased K_m for ATP but unchanged maximal actin-activated ATPase activity or motility (Ruppel et al., 1994). The resultant mutant protein is less stable than the wild type presumably due to the introduction of a hydrophobic residue at the surface of the protein and loss of salt bridge. Thus it is possible that Lys 130 might play an indirect role in stabilizing the conformation of the neighboring residues that form the purine binding site.

The ribose moiety of ADP forms very few specific interactions with the protein or water molecules. However, Asn 127, which is highly conserved, does form a hydrogen bond to the ring oxygen, O4′. The 2′- and 3′-hydroxyl groups are both exposed to solvent, an arrangement that accounts for the observation that a wide variety of functional

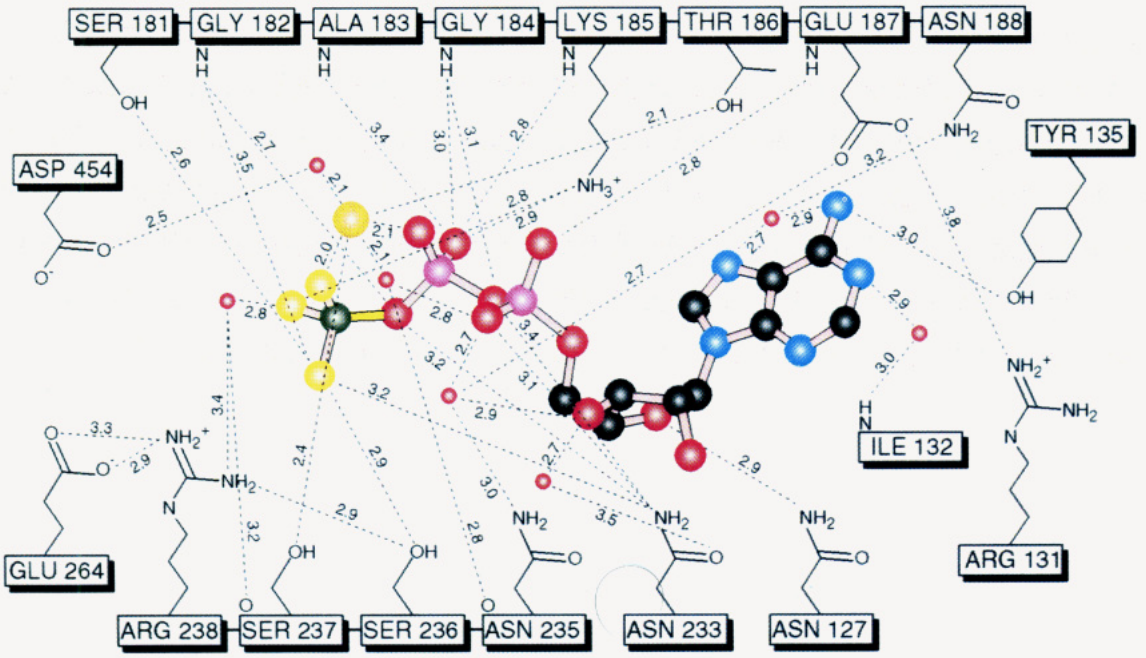

FIGURE 6: Schematic representation of the coordination of the metallofluoride−ADP complex in MgADP•BeF_x•S1Dc. Hydrogen bonds less than 3.5 Å and ionic interactions less than 3.7 Å are shown as dashed lines with the corresponding distances. Only those interactions with the appropriate stereochemistry to participate in these interactions are included. In this figure beryllium, carbon, fluorine, magnesium, nitrogen, oxygen, and phosphorus are depicted in green, black, yellow, orange, blue, red, and pink, respectively.

groups including spin-labels, fluorophores, and photolabels can be attached to the ribose ring in these positions without affecting function (Cole & Yount, 1990; Cremo et al., 1990; Crowder & Cooke, 1987). This accounts for the ability of myosin to utilize organotriphosphates that replace the ribose ring with an aminoethyl group and the purine ring with derivatives of nitrobenzene (Wang et al., 1993).

Structure of the Triphosphate Binding Pocket. The coordination of the α- and β-phosphates is very similar in both MgADP•BeF_x•S1Dc and MgADP•AlF_4•S1Dc. However, there are significant differences between the coordination of the beryllium and aluminum fluoride moieties. The coordination of the α- and β-phosphate and the metallofluoride moiety in the MgADP•BeF_x•S1Dc complex is described first since this mimics the state of the molecule prior to ATP hydrolysis. In the MgADP•BeF_x•S1Dc complex three well-defined peaks of electron density are associated with a terminal oxygen atom of the β-phosphate (Figure 1b). These have been attributed to three fluorine atoms bonded to a beryllium atom. There is little electron density associated with the beryllium since this atom only carries two electrons. Although the coordination surrounding the central beryllium atom is well defined, this study is unable to distinguish between a fluorine or hydroxyl ligand. However, the coordination is consistent with three fluorine ligands. Spectroscopic studies of the beryllium fluoride−ADP adduct with smooth muscle myosin suggest that this complex is a mixture of fluoroberyllates (Henry et al., 1993). The geometry of the heavier atoms and the predicted bond lengths are consistent with an approximately tetrahedral BeF_3O adduct. Furthermore, the predicted beryllium to β-oxygen distance of 1.57 Å is indistinguishable from the bridging oxygen distances between the α- and β-phosphate groups (1.56 and 1.67 Å, respectively). Likewise the Be−F bond distances are similar to the nonbridging P−O bond distances. The MgADP•BeF_x complex is thus an analog of ATP in the active site.

In the MgADP•BeF_x•S1Dc complex the α- and β-phosphate groups and metallofluoride moiety extend down into a narrow tunnel formed by the phosphate binding loop Gly 179 to Val 187 on one side and residues Asn 233 to Gly 240 on the other. This tunnel opens into the apex of the cleft that splits the upper and lower domains of the central 50 kDa segment of the heavy chain. The magnesium ion is located at the top of the tunnel (Figure 5) and is surrounded by six ligands in an approximately octahedral arrangement and plays a central role in chelating the nucleotide complex where it interacts with both the β-phosphate and the BeF_x moiety. The Mg^{2+} ion is also coordinated to two protein ligands, Oγ1 of Thr 186 and Oγ of Ser 237 and two water molecules. These two water molecules are an integral part of the coordination scheme of the nucleotide. One of these water molecules interacts with the carboxyl side chain of Asp 454 and also forms a bond to a fluorine atom of BeF_x. The second interacts with the main-chain carbonyl oxygen of Asn 235 and one of the β-phosphate oxygen atoms.

There are an extensive series of specific interactions between the α- and β-phosphate groups and BeF_x moiety with the protein (Figure 6). Every oxygen and fluorine of the pseudo-triphosphate moiety is involved in a hydrogen-bonding interaction. However, there are more interactions to the β-phosphate and BeF_x moiety than the α-phosphate group. The phosphate binding loop contributes six hydrogen bonds from its main-chain amide nitrogens and additional interactions from the side chains of Ser 181, Thr 186, and Lys 187. The opposite side of the binding pocket formed by residues Asn 233 to Gly 240 contributes six hydrogen bonds from both the backbone and side chains to the β-phosphate and BeF_x moiety either directly or via a buried water molecule. Oγ of Ser 236 is hydrogen-bonded to one of the fluorine atoms. The analogous atom in skeletal muscle myosin was identified previously to be a ligand of the γ-phosphate from photoreaction of the vanadate−ADP complex (Grammer & Yount, 1991).

The bottom of the nucleotide binding pocket abuts the apex of the narrow cleft that splits the 50 kDa segment of the heavy chain. The region around the metallofluoride moiety will be referred to as the γ-phosphate pocket. This pocket contains at least three well-ordered water molecules. One of these forms a short hydrogen bond, 2.5 Å, to one of the fluorine atoms. This water molecule is roughly opposite the phosphate oxygen that forms the pseudobridge to beryllium. It is expected that hydrolysis of ATP occurs through nucleophilic attack of the γ-phosphorus by a water molecule approaching from a direction opposite to the bridging oxygen. The water molecule observed in the MgADP·BeF_x·S1Dc complex is well situated for this purpose. The other water molecules in the γ-phosphate pocket participate in stabilizing the infrastructure surrounding the beryllium fluoride moiety.

The overall coordination of the magnesium ion and α- and β-phosphate groups in MgADP·AlF_4·S1Dc is very similar to that seen in the MgADP·BeF_x·S1Dc complex (Figure 7). Only five ligands are observed for the magnesium ion, whereas six were seen in the beryllium complex. The water molecule that bridges the magnesium ion and Asp 454 in MgADP·BeF_x·S1Dc is not evident in MgADP·AlF_4·S1Dc, even though the disposition of all of the other ligands is identical in both complexes. This difference is most likely due to the lower resolution and less complete refinement in the MgADP·AlF_4·S1Dc complex. The location of the aluminum in the structure of the MgADP·AlF_4·S1Dc complex is unambiguous (Figure 1c). Although the arrangement of ligands is less well defined, due to the resolution of the data, the overall coordination of the metal ion is octahedral. One of the ligands is contributed by an oxygen atom of the β-phosphate. Four of the remaining ligands lie in a plane and are most likely fluorine atoms, which is consistent with spectroscopic studies of this complex in smooth muscle myosin (Maruta et al., 1993). The electron density for the water molecule, axial to the pseudobridging oxygen atom, is not well defined at the present resolution and has not been included in the model. This water molecule would be analogous to that coordinated to the BeFx moiety close to the axial position (Figure 1b). The stereochemistry observed here for the AlF_4^- moiety is similar to that seen in the structures of the G-protein $G_{i\alpha 1}$ and transducin α complexes with guanosine diphosphate (GDP) and aluminum fluoride (Coleman et al., 1994; Sondek et al., 1994). There are several other well-ordered water molecules in the γ-phosphate pocket in locations analogous to those seen in the MgADP·BeF_x·S1Dc structure.

The bond distance to the pseudobridging oxygen is distinctly longer (2.0 Å) in the MgADP·AlF_4·S1Dc complex than in the MgADP·BeF_x·S1Dc (1.57 Å). This change allows one of the fluorine ligands to the aluminum to form a short hydrogen bond to the amide hydrogen of Gly 457, which stabilizes a movement of the main chain by 4.4 Å. Gly 457 is completely conserved in the myosin superfamily. In the MgADP·BeF_x·S1Dc complex the respective fluorine is too far away to form this interaction. Because of the longer bond distance to pseudobridging oxygen observed in the MgADP·AlF_4·S1Dc complex it appears that this complex is an analog of the transition state in comparison to MgADP·BeF_x·S1Dc which more closely mimics the prehydrolysis state (ATP). The MgGDP·AlF_4 structures of the G-protein $G_{i\alpha 1}$ and transducin α complexes were also interpreted as transition state analogs (Coleman et al., 1994; Sondek et al., 1994).

Comparison of the Metallofluoride Complexes. Superposition of four regions (Table 2) of MgADP·BeF_x·S1Dc structure onto the corresponding regions of MgADP·AlF_4·S1Dc and chicken myosin S1 indicates that the overall fold of these parts of the S1 molecule is essentially identical in all of these structures. The rms difference between the MgADP·AlF_4·S1Dc and MgADP·BeF_x·S1Dc structures is 1.5 Å, which results from the partial closure of the narrow cleft in the central 50 kDa segment (Figure 7a). Analysis of the MgADP·AlF_4·S1Dc model superimposed onto MgADP·BeF_x·S1Dc, matching the first part of the central 50 kDa segment, Gly 209 to Asp 454, indicates that the closure results from a concerted rigid-body movement of the lower domain, Gly 457 to Ser 619; the amount of closure is estimated to be about 5°. The overall rms difference between the MgADP·AlF_4·S1Dc and MgADP·BeF_x·S1Dc underestimates the significance of this domain movement, since the outer edge of the cleft moves by more than 5 Å.

The movement is essentially a bending at residues Ile 455 and Gly 457, located at the end of a β-strand which drops from the upper part of the central domain into the lower. The bending at Ile 455 involves a single rotation about the main-chain conformational torsion angle ϕ (the torsion angles ϕ and ψ, are $-152°$ and 155° in MgADP·BeF_x·S1Dc, $-155°$ and 169° in chicken S1, and $-59°$ and 166° in MgADP·AlF_4·S1Dc), while at Gly 457, the change involves the ψ angle ($-70°$ and 136° in MgADP·AlF_4·S1Dc compared to $-89°$ and $-162°$ in MgADP·BeF_x·S1Dc). The conformational torsion angles in residues on either side of this hinge region remain virtually unchanged in all structures; the rms difference in ϕ and ψ angles for five amino acids on either side of Ile 455 (Ile 464 in chicken S1) is $\approx 20°$.

The flexing at Ile 455 and Gly 457 brings the loop from Ser 456 to Ser 465 and the NH_2-terminal region of the following helix (Phe 466 to Cys 470) into close proximity to a region in the upper central domain near the active site. Five new interdomain contacts are introduced: a hydrogen bond from the O_γ of Ser 456 to the carbonyl oxygen of Ser 237, a salt bridge between the side chains of Glu 459 and Arg 238, and hydrogen bonds between the side chains of Glu 467 ($O_{\epsilon 2}$) and Ser 266 (O_γ), and Gln 468 ($N_{\epsilon 2}$) and Glu 264 ($O_{\epsilon 1}$), and between the carbonyl oxygen of Ile 460 and the side chain of Arg 232. In addition, there are water-mediated interactions between the side chains of Ser 181, Thr 230, and Arg 238 ($N_{\eta 2}$) in the upper central domain and Glu 459 ($O_{\epsilon 2}$) in the lower. Finally, there is the direct interaction between the main-chain nitrogen of Gly 457 and one of the fluoride ions of the AlF_4^- moiety.

Movement of the lower domain relative to the upper domain of the central segment of the heavy chain in the MgADP·AlF_4·S1Dc complex is coupled to a structural change in the COOH-terminal domains. These are mediated by the loop extending from Tyr 573 to Gly 575 that abuts the final helix observed in the MgADP·AlF_4·S1Dc complex. This helix separates Cys 678 and Thr 688 that are the equivalent residues to the reactive cysteine residues (SH2 and SH1) in skeletal muscle. A 5 Å movement of Tyr 573 induces an $\sim 20°$ rotation and 2.5 Å translation of that helix relative to its prior location (the change in the disposition of this helix is evident in Figure 4b). Unfortunately, the polypeptide chain beyond Lys 690 in the MgADP·AlF_4·S1Dc complex appears to adopt multiple conformations in the crystal. This lack of conformational stability is most likely due to the absence of

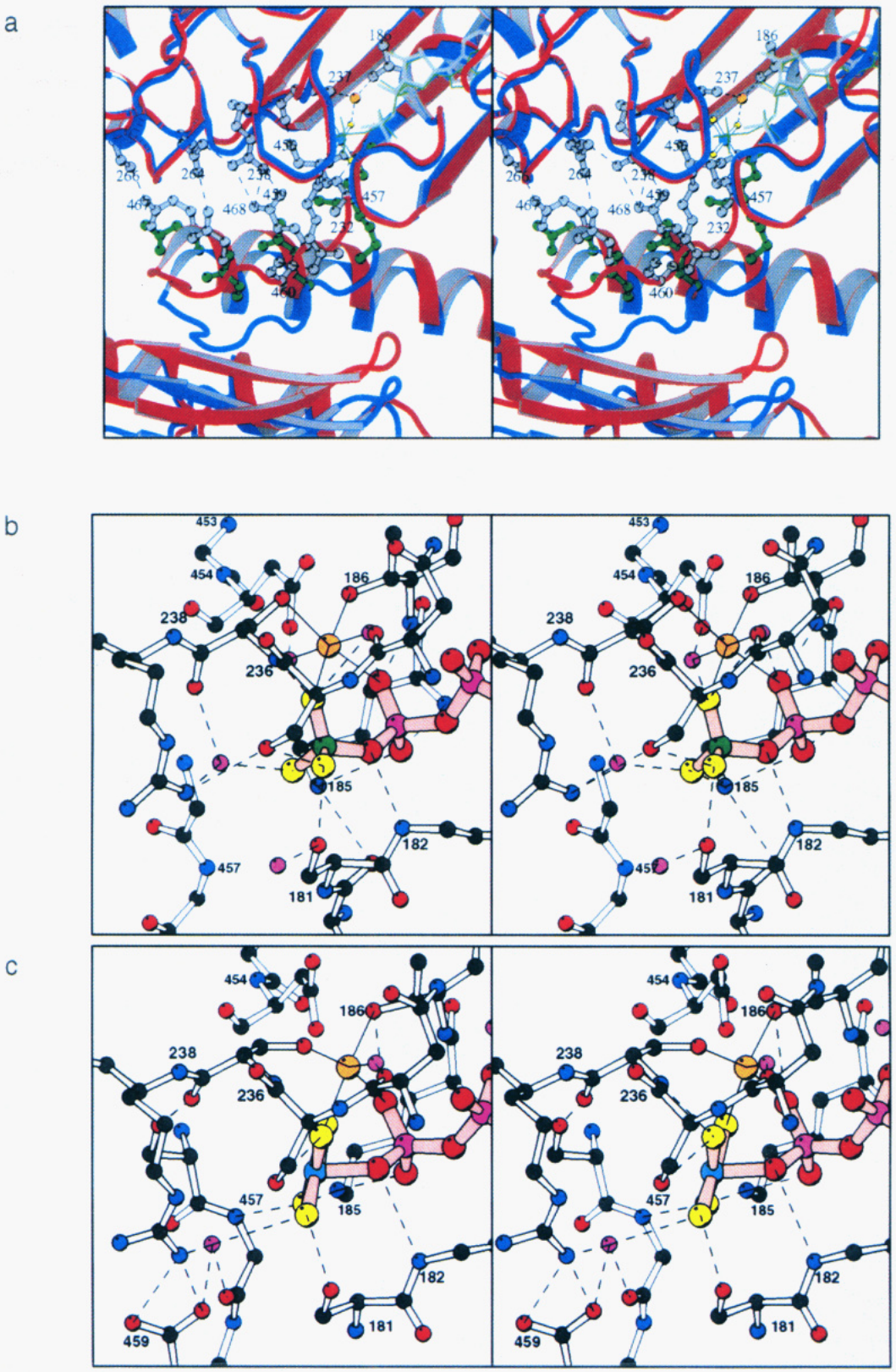

FIGURE 7: Structural differences in the γ-phosphate pockets of the MgADP•BeF_x•S1Dc and MgADP•AlF_4•S1Dc complexes. (a) Tertiary structural differences between the MgADP•BeF_x•S1Dc (blue) and MgADP•AlF_4•S1Dc (red) complexes. The additional interactions between the upper and lower domains of the central segment of the myosin heavy chain prompted by the AlF_4^- ion are included. Side-chain and nucleotide positions in MgADP•AlF_4•S1Dc are shown in gray and their corresponding orientation in MgADP•BeF_x•S1Dc in green. (b) and (c) Close-up views of the interactions of the β-phosphate, metallofluoride ions, and water molecules in the phosphate binding pocket in MgADP•BeF_x•S1Dc and MgADP•AlF_4•S1Dc, respectively.

the essential light chain. This also suggests that a different structural change in the COOH-terminal domain would be observed if the essential light chain was present. As a consequence the current structures are inappropriate to explain the cross-linking of the reactive cysteine residues in skeletal muscle in the presence of ATP (Huston et al., 1988), although they do indicate that this segment of the structure undergoes a conformational change during hydrolysis.

Mechanism of Hydrolysis. Kinetic studies have shown that ATP binding is a multistep process that is followed by rapid hydrolysis, which results in a metastable complex of myosin, ADP, and inorganic phosphate (P_i) (Lymn & Taylor, 1971; Trybus & Taylor, 1982). The equilibrium constant between ATP and ADP,P_i is approximately unity on the enzyme (depending on the ionic strength and pH) (Bagshaw & Trentham, 1973, 1974; Lymn & Taylor, 1971). During this time there is rapid interconversion between substrate and products (Bagshaw & Trentham, 1973; Trentham et al., 1976). Hydrolysis of ATP occurs by attack of a water molecule on the γ-phosphorus.

Although myosin has been studied extensively, very little is known about the role of the protein in ATP hydrolysis. In particular the identity of the catalytic base, if it exists, has not been defined. Examination of the γ-phosphate pocket in both MgADP·BeF_x·S1Dc and MgADP·AlF_4·S1Dc does not reveal any amino acid side chains within 5 Å of the beryllium or aluminum that might function as a catalytic base (Figure 7c). The closest groups to the aluminum are Oγ of Ser 236 (4.0 Å), Oγ of Ser 237 (3.8 Å), Oγ of Ser 181 (4.0 Å), and Nζ of Lys 185 (3.8 Å) (Figure 7b). Additional groups in the γ-phosphate pocket include Glu 459 and Ser 456. Ser 181 lies in the plane of the AlF_4^- ion and is hydrogen-bonded to one of the fluorine ligands. Ser 236 is hydrogen-bonded to one of the fluorine ligands. Ser 237 is coordinated to the magnesium ion and thus cannot function as the base. Likewise Lys 185 is coordinated to both a β-phosphate oxygen and one of the fluorines and would not be expected to function as a base. Glu 459, which is hydrogen-bonded to a water molecule in the γ-phosphate pocket, is too far from the aluminum to function as a base. If a water molecule were included in the coordination sphere for the aluminum, it would be located 3.4 Å from Ser 456. Oγ of Ser 456 is 5.2 Å from the aluminum and directly opposite the pseudo-bridging oxygen of the β-phosphate. There are at least four serine residues associated with the γ-phosphate pocket. However, unless one of these is activated, as in serine proteases, it would not be expected to function as a base. Examination of the structure does not reveal any side chains that might serve to reduce the pK_a of these serine residues. However, all of these residues are completely conserved.

The lack of an obvious candidate for a base suggests that water might function as the nucleophile with direct transfer of its proton to the γ-phosphate. This would eliminate the need for an amino acid side chain to function as the base and would allow the protein to catalyze the reaction by stabilizing a trigonal-planar arrangement of oxygen ligands around the γ-phosphorus atom at the transition state. A similar mechanism has been suggested previously for transducin α (Sondek et al., 1994) and $p21^{ras}$ (Schweins et al., 1995) Alternatively, one of the serine residues associated with the γ-phosphate pocket might serve as an intermediate in the transfer of the proton from the nucleophilic water molecule to the γ-phosphate (Figure 8). In this alternative mechanism, the serine would participate in hydrogen exchange but would not function as a catalytic base. The rate constant for the bond cleavage step in ATP hydrolysis by myosin is approximately 5 s^{-1} at 3 °C (Taylor, 1977) and is smaller than the minimum rate of hydrogen exchange of 30 s^{-1} for serine hydroxyl protons as measured by NMR at 4 °C (Liepinsh et al., 1992). The latter occurs in neutral solution at pH 6.5 in model peptides; however, the exchange

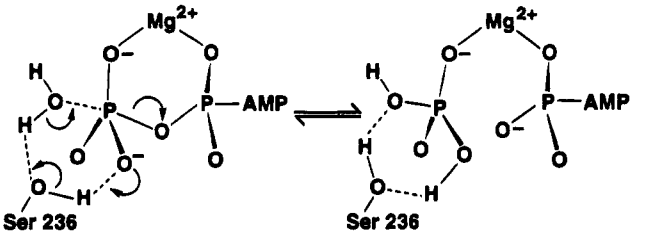

FIGURE 8: Proposed mechanism of hydrolysis for myosin where Ser 236 acts as an intermediary in the proton transfer from the hydrolytic water molecule to the γ-phosphate.

rate would be considerably higher in the polar environment of the γ-phosphate pocket. A possible candidate for this type of proton transfer is Ser 236. In both complexes, Oγ of Ser 236 is coordinated to one of the fluorine atoms and is situated appropriately for interaction with the anticipated incoming water molecule. This mechanism would provide better stereochemistry for proton transfer from the incoming water to the γ-phosphate than direct transfer.

Myosin is unusual in that it forms a metastable state (ADP,P_i) after hydrolysis. In the absence of actin, product release is slow. Kinetic studies have shown that there is no release of protons during the bond cleavage (Bagshaw & Trentham, 1973) and that this occurs at the time of product release. Furthermore, ^{18}O exchange studies have suggested that the phosphate group of the product is tumbling rapidly in the active site since all of the nonbridge phosphate oxygen atoms are equivalent (Bowater et al., 1990; Trentham et al., 1976). The cavity associated with the putative location of the γ-phosphate is large enough to accommodate a phosphate group and contains sufficient hydrogen bond donors and acceptors to coordinate this ion. In the MgADP·AlF_4·S1Dc complex, which mimics the transition state for hydrolysis, there is reduced access of solvent to the γ-phosphate pocket caused by partial closure of the cleft. If this conformational change is maintained in the metastable ADP,P_i state, it provides a structural explanation for the kinetic stability this state.

Kinetic studies indicate that the phosphate ion is released prior to ADP during the contractile cycle (Goldman, 1987; Trentham et al., 1976). The arrangement of MgADP and the metallofluoride in both structures suggests the phosphate ion cannot leave via the same route that the substrate enters. It is unlikely that the phosphate ion could squeeze past MgADP. The kinetic data and X-ray structures indicate that phosphate may depart from the bottom of the active site pocket as has been suggested from modeling ATP in the active site of myosin (Yount et al., 1995).

The original model for the contractile cycle derived from the structure of chicken skeletal muscle myosin S1 suggested that the nucleotide pocket closed when ATP bound to generate a bent molecule (Rayment et al., 1993a). An assumption was made that the conformation of chicken skeletal myosin S1 observed in that structure was intermediate between the actin and ATP-bound state of the molecule. The structure of the MgADP·BeF_x·S1Dc complex indicates that the motor unit of chicken skeletal myosin S1 when methylated and crystallized from ammonium sulfate is essentially identical to the ATP-bound state. There are several ways to interpret this observation. First, the conformation of myosin S1 in solution might be closer to the nucleotide-bound state. This would then account for the very

high binding constant of myosin for ATP and would explain the difficulty of detecting any major macroscopic change in its structure upon addition of ATP with most physical techniques. Alternatively, the structure of the chicken S1 might be a function of the methylation or the high concentration of ammonium sulfate that is known to be a competitive inhibitor of ATP binding (Tesi et al., 1988). Indeed, a sulfate ion was observed in the nucleotide pocket of the chicken S1 structure (Rayment et al., 1993b). It is difficult to separate these possibilities. However, it would appear from these structural studies that closure of the nucleotide pocket is not the source of the major conformational change that is responsible for the molecular basis of muscle contraction. This is consistent with recent fluorescence quenching measurements, which show that the purine base of adenine experiences a similar environment at the beginning and end of the contractile cycle (Franks-Skiba et al., 1994). The structures of the beryllium and aluminum fluoride complexes suggest that movements in the myosin heavy chain associated with the lower domain of the central 50 kDa segment coupled to movements in the COOH-terminal segment are the primary source of this conformational change. The implications of this modification to the structural model for the contractile cycle have been discussed elsewhere (Fisher et al., 1995).

CONCLUSION

The structure of the truncated myosin head from *Dictyostelium* is remarkably similar to that of chicken skeletal myosin S1 considering that both light chains are missing from the former structure. The differences between the NH_2- and COOH-terminal segments of MgADP·BeF_x·S1Dc and MgADP·AlF_4·S1Dc reported here re-emphasize the importance of the essential light chain in energy transduction (Lowey et al., 1993). It has been suggested that the light chain binding motif serves to amplify the conformational changes in the head and increase the size of the power stroke (Rayment et al., 1993b). This has been substantiated by genetic experiments that removed the binding site for the regulatory light chain (Uyeda & Spudich, 1993). However, it now appears that the interactions between the essential light chain and the motor unit are important for transmitting the conformational changes induced by ATP binding and hydrolysis to the remainder of the molecule. This is consistent with the observation that a significant fraction of mutations in β-cardiac myosin that have been implicated in familial hypertrophic cardiomyopathy map to the interface between the essential light chain and the heavy chain (Rayment et al., 1995).

The current structural results emphasize the importance of the narrow cleft that splits the central 50 kDa segment of the heavy chain. They further suggest that it not only functions in sensing the presence of the γ-phosphate of ATP but also is responsible for transducing the conformational change that results in the power stroke. The new information derived from the structure of the truncated *Dictyostelium* head shifts the location of the conformational change in the structural hypothesis from the nucleotide binding pocket to the region associated with the reactive cysteine residues. This is consistent with the chemical evidence that implicates conformational changes in this region during the hydrolytic process (Burke & Reisler, 1977; Dalbey et al., 1983; Wells & Yount, 1980). These new structural results provide further evidence that actomyosin-based motility is driven by conformational rearrangement of domains.

ACKNOWLEDGMENT

We thank G. H. Reed for helpful discussions and W. W. Cleland for suggesting the potential role of serine in the hydrolytic mechanism. We thank Siemens (Madison) for the loan of a HI-STAR double detector system used in this study.

REFERENCES

Bagshaw, C. R., & Trentham, D. R. (1973) *Biochem. J. 133*, 323–328.
Bagshaw, C. R., & Trentham, D. R. (1974) *Biochem. J. 141*, 331–349.
Balint, M., Sreter, F. A., Wolf, I., Nagy, B., & Gergley, J. (1975) *J. Biol. Chem. 250*, 6168–6177.
Bivin, D. B., Ue, K., Khoroshev, M., & Morales, M. F. (1994) *Proc. Natl. Acad. Sci. U.S.A. 91*, 8665–8669.
Bowater, R., Zimmerman, R. W., & Webb, M. R. (1990) *J. Biol. Chem. 265*, 171–176.
Brünger, A. T. (1990a) *Acta Crystallogr. A46*, 46–57.
Brünger, A. T. (1990b) *X-PLOR Version 3.1: A System for Crystallography and NMR*, Yale University, New Haven, CT.
Burke, M., & Reisler, E. (1977) *Biochemistry 16*, 5559–5563.
Chothia, C., & Lesk, A. M. (1986) *EMBO J. 5*, 823–826.
Cole, D., & Yount, R. G. (1990) *J. Biol. Chem. 265*, 22547–22546.
Coleman, D. E., Berghuis, A. M., Lee, E., Linder, M. E., Gilman, A. G., & Sprang, S. R. (1994) *Science 265*, 1405–1412.
Cooke, R. (1986) *CRC Crit. Rev. Biochem. 21*, 53–118.
Cremo, C. R., Neuron, J. M., & Yount, R. G. (1990) *Biochemistry 29*, 3309–3319.
Crowder, M. C., & Cooke, R. (1987) *Biophys. J. 51*, 323–333.
Dalbey, R. E., Weiel, J., & Yount, R. G. (1983) *Biochemistry 22*, 4696–4706.
Fisher, A. J., Smith, C. A., Thoden, J., Smith, R., Sutoh, K., Holden, H. M., & Rayment, I. (1995) *Biophys. J. 68*, 19s-28s.
Franks-Skiba, K., Hwang, T., & Cooke, R. (1994) *Biochemistry 33*, 12720–12728.
Goldman, Y. E. (1987) *Ann. Rev. Physiol. 49*, 637–654.
Goodno, C. C. (1982) in *Methods in Enzymology* (Frederiksen & Cunningham, Eds.) pp 116–123, Academic Press, New York.
Grammer, J. C., & Yount, R. G. (1991) *Biophys. J. 59*, 226a.
Henry, G. D., Maruta, S., Ikebe, M., & Sykes, B. D. (1993) *Biochemistry 32*, 10451–10456.
Holmes, K. C., Popp, D., Gebhard, W., & Kabsch, W. (1990) *Nature 347*, 44–49.
Huston, E. E., Grammer, J. C., & Yount, R. G. (1988) *Biochemistry 27*, 8945–8952.
Huxley, A. F., & Niedergerke, R. (1954) *Nature 173*, 971–973.
Huxley, H., & Hanson, J. (1954) *Nature 173*, 973–976.
Itakura, S., Yamakawa, H., Toyoshima, Y. Y., Ishijima, A., Kojima, T., Harada, Y., Yamnagida, T., Wakabayashi, T., & Sutoh, K. (1993) *Biochem. Biophys. Res. Commun. 196*, 1504–1510.
Jones, T. A. (1985) in *Methods in Enzymology* (Wycoff, H. W., Hirs, C. H. W., & Timasheff, S. N., Eds.) pp 157–171, Academic Press Inc., New York.
Kabsch, W., Mannherz, H. G., Suck, D., Pai, E. F., & Holmes, K. C. (1990) *Nature 347*, 37–44.
Kraulis, P. J. (1991) *J. Appl. Crystallogr. 24*, 946–950.
Liepinsh, E., Otting, G., & Wüthrich, K. (1992) *J. Biomol. NMR 2*, 447–465.
Lowey, S., Waller, G. S., & Trybus, K. M. (1993) *Nature 365*, 454–456.
Lundblad (1991) *Chemical Reagents for Protein Modification*, 2nd ed., CRD Press, Boca Raton, FL.
Lymn, R. W., & Taylor, E. W. (1971) *Biochemistry 10*, 4617–4624.
Manstein, D. J., Titus, M. A., De-Lozanne, A., & Spudich, J. A. (1989) *EMBO J. 8*, 923–932.
Maruta, S., Henry, G. D., Sykes, B. D., & Ikebe, M. (1993) *J. Biol. Chem. 268*, 7093–7100.
Means, G. E., & Feeney, R. E. (1968) *Biochemistry 7*, 2192–2201.

Milligan, R. A., & Flicker, P. F. (1987) *J. Cell Biol. 105*, 29−39.
Milligan, R. A., Whitaker, M., & Safer, D. (1990) *Nature 348*, 217−221.
Mornet, D., Pantel, P., Audemard, E., & Kassab, R. (1979) *Biochem. Biophys. Res. Commun. 89*, 925−932.
Muller, C. W., & Schulz, G. E. (1992) *J. Mol. Biol. 224*, 159−177.
Navaza, J. (1993) *Acta Crystallogr. D49*, 588−591.
Pai, E. F., Krengel, U., Petsko, G. A., Goody, R. S., Kabsch, W., & Wittinghofer, A. (1990) *EMBO J. 9*, 2351−2359.
Pate, E., Franks-Skiba, K., White, H., & Cooke, R. (1993) *J. Biol. Chem. 268*, 10046−10053.
Phan, B., & Reisler, E. (1992) *Biochemistry 31*, 4787−4793.
Phan, B. C., Faller, L. D., & Reisler, E. (1993) *Biochemistry 32*, 7712−7719.
Phan, B. C., Cheung, P., Miller, C. J., Reisler, E., & Muhlrad, A. (1994) *Biochemstry 33*, 11286−11295.
Rayment, I., Holden, H. M., Whittaker, M., Yohn, C. B., Lorenz, M., Holmes, K. C., & Milligan, R. A. (1993a) *Science 261*, 58−65.
Rayment, I., Rypniewski, W. R., Schmidt-Bäse, K., Smith, R., Tomchick, D. R., Benning, M. M., Winkelmann, D. A., Wesenberg, G., & Holden, H. M. (1993b) *Science 261*, 50−58.
Rayment, I., Holden, H. M., Sellers, J. R., Fananapazir, L., & Epstein, N. D. (1995) *Proc. Natl. Acad. Sci. U.S.A. 92*, 3864−3868.
Read, R. J. (1986) *Acta Crystallogr. A42*, 140−149.
Rossmann, M. G. (1972) *The Molecular Replacement Method*, Gordon and Breach, New York.
Ruppel, K. M., Uyeda, T. Q. P., & Spudich, J. A. (1994) *J. Biol. Chem. 269*, 18773−18780.
Rypniewski, W. R., Holden, H. M., & Rayment, I. (1993) *Biochemistry 32*, 9851−9858.
Schweins, T., Geyer, M., Scheffzek, K., Warshel, A., Kalbitzer, H. R., & Wittinghofer, A. (1995) *Struct. Biol. 2*, 36−44.
Smith, T. J. (1993) *J. Appl. Crystallogr. 26*, 496−498.
Sondek, J., Lambright, D. G., Noel, J. P., Hamm, H. E., & Sigler, P. B. (1994) *Nature 372*, 276−279.
Taylor, E. W. (1977) *Biochemistry 16*, 732−740.
Tesi, C., Barman, T., & Travers, F. (1988) *FEBS Lett. 236*, 256−260.
Tong, L., & Rossmann, M. G. (1990) *Acta Crystallogr. A46*, 783−792.
Tong, S. W., & Elzinga, M. (1983) *J. Biol. Chem. 258*, 13100−13110.
Trentham, D. R., Eccleston, J. F., & Bagshaw, C. R. (1976) *Q. Rev. Biophys. 9*, 217−281.
Tronrud, D. E., Ten Eyck, L. F., & Matthews, B. W. (1987) *Acta Crystallogr. A43*, 489−501.
Trybus, K. M., & Taylor, E. W. (1982) *Biochemistry 21*, 1284−1294.
Uyeda, T. Q. P., & Spudich, J. A. (1993) *Science 262*, 1867−1870.
Walker, J. E., Saraste, M., Runswick, M. J., & Gay, N. J. (1982) *EMBO J. 1*, 945−951.
Wang, D., Pate, E., Cooke, R., & Yount, R. (1993) *J. Muscle Res. Cell Motil. 14*, 484−497.
Warrick, H. M., De Lozanne, A., Leinwand, L. A., & Spudich, J. A. (1986) *Proc. Natl. Acad. Sci. U.S.A. 83*, 9433−9437.
Wells, J. A., & Yount, R. G. (1980) *Biochemistry 19*, 1711−1717.
Werber, M. M., Peyser, M., & Muhlrad, A. (1992) *Biochemistry 31*, 7190−7197.
White, H. D., Belknap, B., & Jiang, W. (1993) *J. Biol. Chem. 268*, 10039−10045.
White, H. W., & Rayment, I. (1993) *Biochemistry 32*, 9859−9865.
Xie, X., Harrison, D. H., Schlichting, I., Sweet, R. M., Kalabokis, V. N., Szentz-Gyorgyi, A. G., & Cohen, C. (1994) *Nature 368*, 306−312.
Yount, R. G., Cremo, C. R., Grammer, J. C., & Kerwin, B. A. (1992) *Philos. Trans. R. Soc. London B336*, 55−61.
Yount, R. G., Lawson, J. D., & Rayment, I. (1995) *Biophys. J.* (in press).

BI950582A